Fangtao *et al. Geoenvironmental Disasters* (2023) 10:27
https://doi.org/10.1186/s40677-023-00257-2

Geoenvironmental Disasters

RESEARCH

Open Access

Evaluation of the collapsible deformation of surrounding rock of loess hydraulic tunnel considering ground stress variation

She Fangtao[1,2,3*], Xu Wanying[1], Liu Lele[1], Liu Guoping[4], Li Lei[4] and Duan Changhui[5]

Abstract

Background Uneven settlement will occur as a result of the collapsible deformation of the loess strata, and the hydraulic tunnel lining structure will also fail. In this work, laterally confined compression tests were carried out on loess and the double-line method was employed to evaluate the loess collapsibility. The deformation of the surrounding rock of a loess hydraulic tunnel under various ground stresses and its effect on the lining structure was modeled.

Results Three stages were noted in the collapsible deformation of loess. The critical point between the former two stages corresponds to the pre-consolidation pressure of saturated loess and that between the latter two is taken as the structural yield pressure of unsaturated loess.

Conclusion From the relationship between the collapsibility coefficient and vertical stress, the deformation of the tunnel under ground seepage primarily originates from two sources, i.e., the collapsible and compressive deformation. The latter source accounts for the deformation of loess adjacent to the lining when the seepage depth is low, while both sources are included when the bottom of the tunnel invert is infiltrated. The collapsible deformation is lower than that of the original stratum due to the stress relaxation during tunnel excavation. The tensile and compressive stresses of tunnel lining increase linearly with the seepage depth, with the maximum appearing at a position of 20 m away from the midline of the collapse and non-collapse domains. The results will provide a theoretical reference to the design and construction of hydraulic tunnels in collapsible loess stratum.

Keywords Loess collapsibility, Double-line method, Collapsibility coefficient, Hydraulic tunnel, Ground stress

Introduction

Around 6.6% of the land area in China is covered with loess, including the Songliao Plain in the northeast, north China, and the northwest, mainly found in the inland region between 34° and 41°N. We commonly refer to the contiguous loess region that stretches from the Wushaoling Mountains in the west to the Taihang Mountains in the east, and from the Great Wall in the north to the Qinling Mountains in the south as the Loess Plateau of China (Li et al. 2016a; Derbyshire 2001). The Late Pleistocene (Q_3) loess in this region is characterized by loose texture, large cracks, and the presence of vertical joints (Derbyshire et al. 1995; Haeri et al. 2016). The soil has a relatively low dry bulk density, large pore size, significant

*Correspondence:
She Fangtao
shefangtao@xaut.edu.cn
[1] Institute of Geotechnical Engineering, Xi'an University of Technology, Xi'an 710048, China
[2] Shaanxi Key Laboratory of Loess Mechanics and Engineering, Xi'an 710048, China
[3] State Key Laboratory of Eco-Hydraulics in Northwest Arid Region, Xi'an University of Technology, Xi'an 710024, Shaanxi, China
[4] Hanjiang to Weihe River Valley Water Diversion, Project Construction Co., Ltd., Xi'an 710024, Shaanxi, China
[5] Changzhi City River Affairs Center, Changzhi 046000, Shanxi, China

compressibility, high permeability, and relatively low structural strength. It is highly influenced by water infiltration, exhibiting collapsibility or strong collapsibility, and is considered the main geological formation for the burial of collapsible loess (Weng et al. 2021). It is frequently utilized as a construction material or as a foundation soil. Improper handling of this particular type of soil often results in significant incidents of subsidence or collapse accidents (Smalley et al. 2001; Haeri et al. 2019; Houston et al. 1988).

With the development of underground spaces in western regions of China, a growing number of tunnels must pass through loess layers. Tunnel safety will be put at risk due to the intrinsic collapsibility of loess and will also suffer structural damage when passing through the self-weight collapsing loess layer due to the combined effects of water infiltration and ground subsidence (Shao et al. 2013). The self-weight collapsibility and the collapsible deformation of the loess layers can be introduced to evaluate the stability of the loess tunnel (Sharma and Singhal 2012; Reznik 2007). These characteristics can also be approximated by referencing the site subsidence classification in the Code for Construction in Collapsible Loess Areas (GB 50025-2018). Two research methodologies are employed to investigate loess collapsibility deformation: theoretical calculation and field pit immersion test. Weng et al. (2019) conducted centrifugal model tests to analyze the influence of non-uniform collapsibility of loess on the deformation and failure of tunnel structures. Shao et al. (2017) discussed the railway subgrade settlement control standard based on numerical computation and categorized tunnel foundation collapsible deformation into three grades. Li et al. (2019) carried out large-scale field pit immersion testing, emphasizing the importance of properly accounting for the reduction in bearing capacity and foundation settlement at the tunnel arch foot induced by immersion during the design and construction phases. The above studies provide a valuable reference for revealing the mechanism of collapsible deformation of loess surrounding rock and ensuring the safe construction of loess tunnels.

Irrigation and water diversion projects that involve a significant number of hydraulic tunnels pass through the loess stratum. However, the current studies on loess tunnels are mainly focused on railway and highway tunnels, with less attention to hydraulic tunnels. The water conservancy tunnel project in the collapsible loess stratum is more based on the relevant research results of buildings, channels, and tunnels (Li et al. 2016b), or more concerned with the physical and mechanical properties of collapsible loess itself (Su 2019). It has not formed a set of calculation and analysis methods for collapsible deformation of tunnel foundation from laboratory test, theoretical analysis to numerical simulation. Besides, the existing specifications do not address the design considerations for collapsible loess tunnels in hydraulic structures, and there are few specific guidelines available for such cases. It is critical to take internal water pressure into account for hydraulic tunnels. Collapsible loess is highly susceptible to disturbances such as water infiltration, which may have a detrimental effect on the stability of the surrounding rock and lining structures (Xiao et al. 2022). The superposition method (Li 2007), the unit elimination method (Zhao 2019), the hydraulic equivalent method (Yuan et al. 2017), and the modulus reduction method (Jin et al. 2021) are the four primary calculation methods for studying the deformation properties of collapsible loess in the loess stratum (Liu et al. 2004; Xiao and Tang 2013).

This study aims to evaluate the influence of loess collapsibility on the deformation and even failure of a hydraulic tunnel buried in the loess stratum under various ground stresses. The laboratory unloading collapsible tests were carried out to investigate the collapsible deformation of loess under various vertical stresses (Umar and Sadrekarimi 2016). The relationship between the loess collapsibility coefficient and the increment of vertical compressive stress was established based on the modulus reduction method (Zhi et al. 2021). The collapsible deformation of the surrounding rock of the hydraulic tunnel and its influence on the lining structure were numerically modeled. The results of this study will contribute to the safer and more rational design and construction of hydraulic tunnels in areas with collapsible loess deposits.

Collapsible deformation characteristics of loess

Physical properties of loess

The loess samples were collected from Xi'an, which is one of the typical areas of the Loess Plateau in China. The sampling site is located on Xingfu Road, south of the Longhai Railway and west of the Chan River. The sampling depth is 8 m below the ground surface, and the sampled soil layer is identified as Q_3 loess. The average natural water content of the loess is 20.0%, with a dry density of 1.39 g/cm^3. The basic physical indexes of loess were determined based on the Stand for geotechnical testing method (GB/T 50123-2019), as listed in Table 1.

Test scheme

For engineering design, the coefficient of collapsibility is a critical index to evaluate the settlement and bearing capacity of the loess foundation. The coefficient of collapsibility, as defined by the Code for Building Foundations in Collapsible Loess Areas (GB50025-2018), is the additional settlement per unit thickness of a soil sample saturated with water under a specific pressure. Based

Table 1 Physical indexes of loess

Dry density ρ_d (g/cm^3)	Natural water content w_0 (%)	Plastic limit w_P (%)	Liquid limit w_L (%)	Plasticity index I_P	Specific gravity G_s	Initial void ratio e_0
1.39	20.0%	20.6	31.7	11.1	2.70	0.94

on the laboratory test or field immersion test, there are two main methods commonly used to determine the coefficient of collapsibility: the single-line method and the double-line method. For the former method, the vertical stress is incrementally applied to the sample with the consolidation device until the target pressure is saturated with distilled water. The incremental deformation of the sample after saturation is recorded. The latter method involves two soil samples with one subjected to incremental pressure while the other is saturated with water on the consolidation device and subjected to the same pressure sequence. The double-line method was employed in this study following the Code for Building Foundations in Collapsible Loess Areas (GB 50025-2018). The intact loess blocks wrapped with plastic bags were obtained from the sampling site. The undisturbed cutting-ring samples with different water contents were prepared by titration method and air-drying method, while the saturated samples by the vacuum saturation method. The collapsibility coefficient was determined by the confined compression test with the double-line method. According to the initial water content and saturated water content of the undisturbed samples, the initial water content of the sample was set at 15.0%, 20.0%, 25.0%, and 33.4% (saturated), respectively. The relationship between compressive stress and compressive deformation of samples with different initial water content was then obtained by tests (Fig. 1).

Calculation method of collapsible deformation of loess

Collapsible deformation of loess

Figure 2a illustrates the void ratio e versus vertical pressure p relationship for loess at various initial water contents. When the initial water content is high, the compressive deformation increases significantly at the initial stage with the increase of vertical stress and later stabilizes. Conversely, when the initial water content is low, the compressive deformation exhibits a slower growth increment and reaches a stable state. The yield stress of the structure is defined as the vertical stress corresponding to the inflection point on the e–p curve of the undisturbed soil. From the e–lg$p$ compression curves of different water contents in Fig. 2b, it is evident that when the vertical stress is below the structural yield pressure, the deformation remains in the elastic deformation stage. Otherwise, the soil structure tends to be damaged and the deformation enters the plastic deformation stage. Furthermore, when the considered maximum vertical stress is reached, the void ratio approaches a constant value, indicating that the soil structure tends towards a stable state under the influence of high stress. For samples with varying initial water content, the yield pressure decreases as the initial water content increases. Figure 2c illustrates the relationship between the collapsibility coefficient and vertical stress. The collapsibility coefficient of loess increases linearly with the increase in vertical stress that is below the yield pressure of the

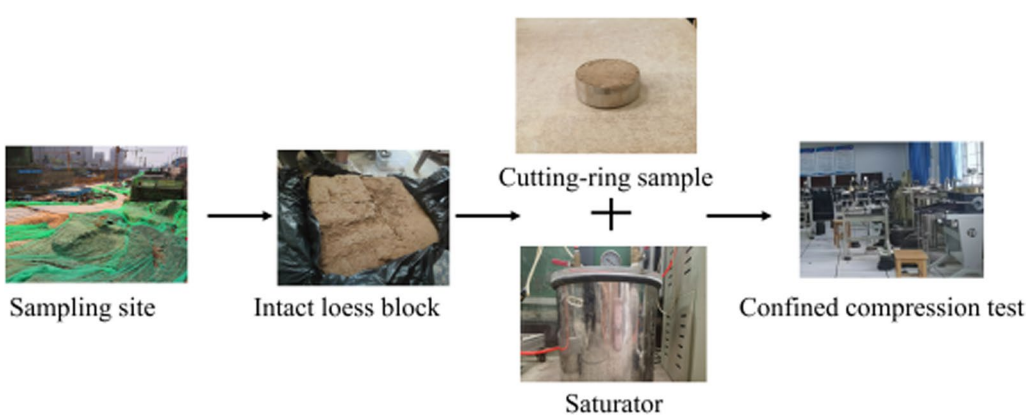

Fig. 1 Soil sample preparation flow chart

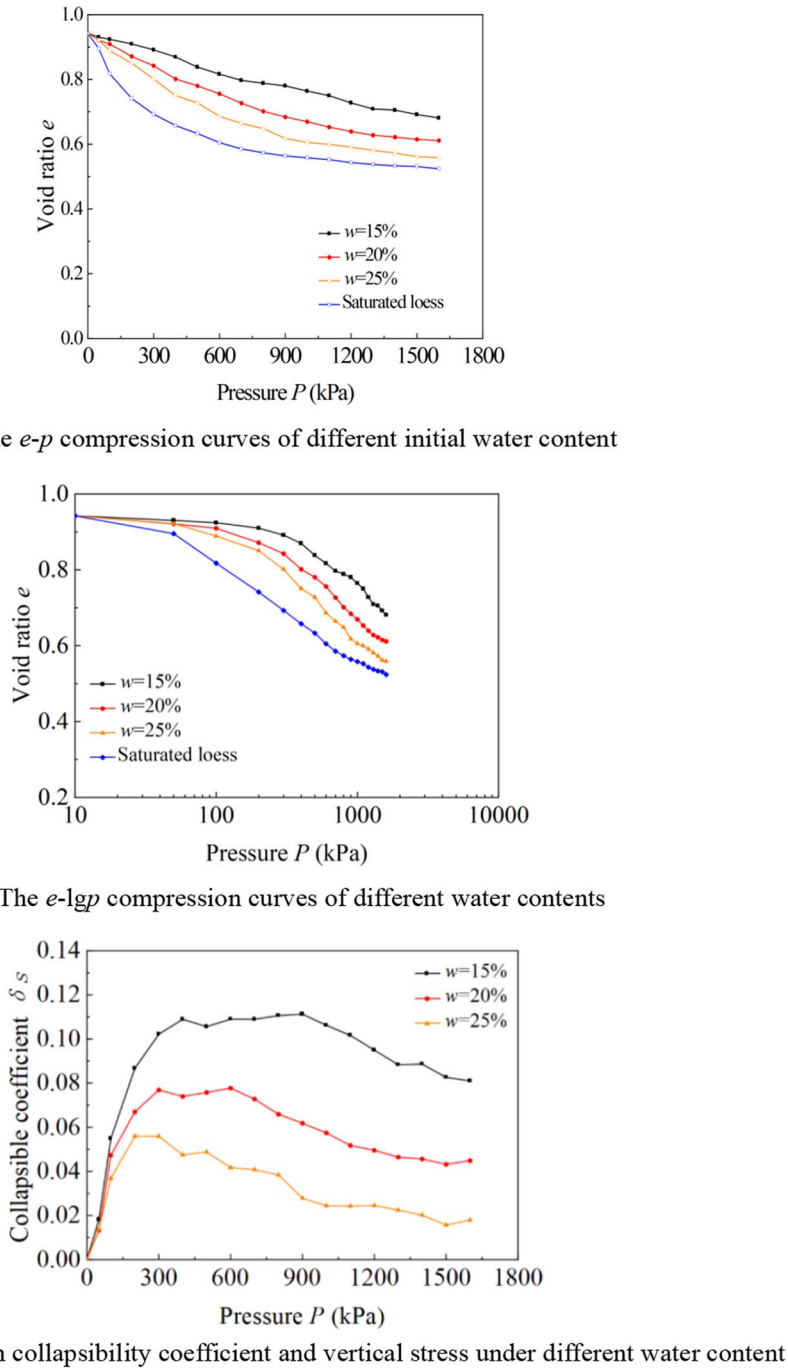

Fig. 2 The void ratio versus vertical stress relationship for loess at various initial water contents

saturated soil structure. In this stage, under increasing load and immersion conditions, the soil sample undergoes elastic deformation, without any damage to the soil structure, resulting in minimal deformation. When the vertical stress exceeds the yield pressure of the saturated soil structure but remains below the yield pressure of the unsaturated soil structure, the collapsibility coefficient increases non-linearly with the increasing vertical stress. In this range, the soil structure is not damaged under the increasing load, but it may experience damage under immersion conditions. However, when the vertical stress exceeds the yield pressure of the unsaturated soil structure, the collapsibility coefficient decreases at greater vertical stress. Under the influence of increasing

load, the soil structure undergoes damage. On the other hand, when subjected to soaking, the adjustment of the soil structure is limited, resulting in relatively small deformation.

Calculation method

The modulus, as a crucial measure of material stiffness, describes the deformation resistance of the material under applied stress. Since the primary concern is the magnitude of collapsible deformation rather than providing a complete stress–strain relationship under wet-load conditions, a calculation method can be developed based on the concept of the double-line method. The double-line method involves comparing the stress–strain curves of the material under natural moisture and saturated conditions at a specific stress state. By examining the difference between these two curves, the extent of collapsible deformation can be determined. This approach focuses on capturing the specific behavior of the loess material during the collapsible process, allowing for a more targeted analysis of the deformation characteristics. It is important to note that the selection of the appropriate modulus and the accurate characterization of the stress–strain relationship is crucial for obtaining reliable results in loess collapsibility simulations. These simulations play a significant role in understanding the potential risks and designing appropriate engineering measures to mitigate the effects of collapsible deformation.

Figure 3 illustrates the schematic diagram of the determination of the collapsibility coefficient from the *e*–lg*p* curve based on the double-line method. According to the method of determining the pre-consolidation pressure by Casagrande (Umar and Sadrekarimi 2016), point B is the structural yield point of the saturated soil sample, and P_{sc} is its corresponding yield pressure. Similarly, point C is the structural yield point of soil samples with natural moisture content, and P_{oc} is the corresponding yield pressure. In this figure, the original height of the sample is denoted as H, and the corresponding initial void ratio is represented as e_0. Under the vertical stress p, the compressive deformation of the sample with natural water content is denoted as s_2, and the corresponding void ratio is e_2. Similarly, the compression deformation of the sample with saturated water content is denoted as s_1, and the corresponding void ratio is e_1. According to the definition of the collapsibility coefficient, it can be expressed as:

$$\delta_s = \frac{s_2 - s_1}{h_0} = \frac{\Delta s}{h_0} = \varepsilon_{sh} \tag{1}$$

The coefficient of collapsibility δ_s represents the collapsible strain ε_{sh} of loess caused by soaking, which is the collapsible deformation per unit height of the sample. In Fig. 4, the compression index, compression modulus, and rebound index of the soil with natural water content are denoted as C_{c2}, E_{s2}, and C_{e2}, respectively. Similarly, the compression index, compression modulus, and rebound index of the saturated soil are denoted as C_{c1}, E_{s1}, and C_{e1}, respectively. The compressive deformation of loess with natural water content s_2 can be calculated by Eq. (2), while that with saturated water content by Eq. (3). The vertical stress increment can be calculated by Eq. (4).

$$s_1 = \frac{C_{e1}}{1+e_0} h_0 \lg\left(\frac{p_{oc}}{p_{sc}}\right) + \frac{C_{c1}}{1+e_0} h_0 \lg\left(\frac{p}{p_{oc}}\right) = \frac{\Delta p h_0}{E_{s1}} \tag{2}$$

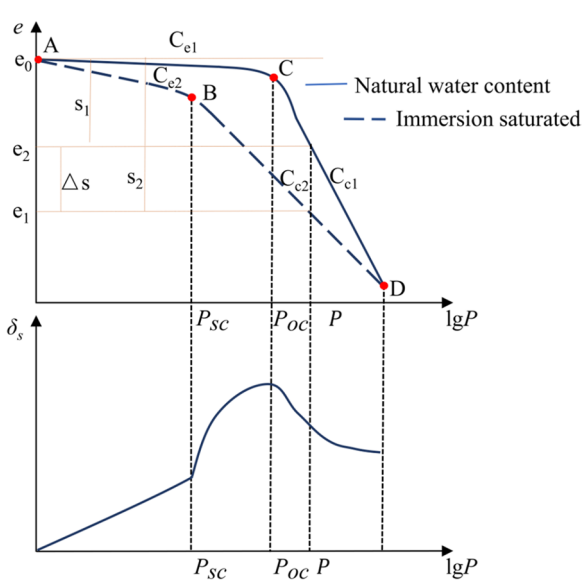

Fig. 3 Schematic diagram of the determination of the collapsibility coefficient from the *e*–lg*p* curve

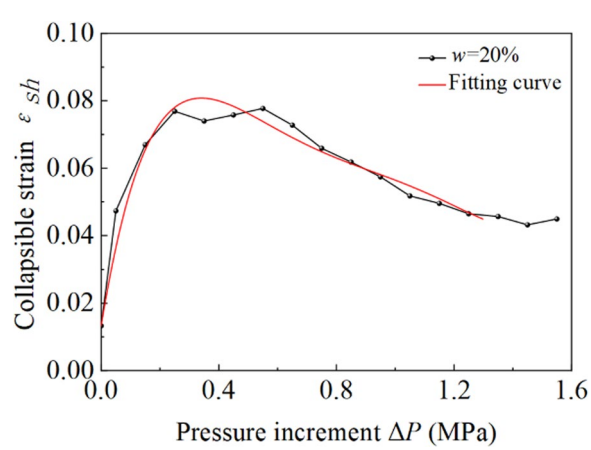

Fig. 4 Fitting curve between the collapsibility coefficient and the vertical stress increment

$$s_2 = \frac{C_{c2}}{1+e_0} h_0 \lg\left(\frac{p}{p_{sc}}\right) = \frac{\Delta p h_0}{E_{s2}} \tag{3}$$

$$\Delta p = p - p_{sc} \tag{4}$$

By substituting Eqs. (2) and (3) into Eq. (1), we obtain:

$$\delta_s = \varepsilon_{sh} = \Delta p \cdot E_{sh} \tag{5}$$

The collapsible secant modulus E_{sh} is defined by:

$$E_{sh} = \frac{E_{s1} \cdot E_{s2}}{E_{s1} - E_{s2}} \tag{6}$$

E_{sh} represents the collapsibility strain $\varepsilon_{\mathrm{sh}}$ induced by immersion under the vertical stress increment Δp, reflecting the ease or difficulty of loess collapsibility under a certain pressure. A smaller collapsible secant modulus indicates a greater collapsibility deformation, and vice versa. The compressibility indexes C_{c2} and C_{c1} are taken as constants, while the compression moduli E_{s1} and E_{s2} are not constant. Therefore, the collapsible secant modulus is not a constant but a parameter that varies with vertical stress, as shown in Fig. 4. Based on the data obtained from the two-line method collapsibility test, the relationship between the collapsibility coefficient and the vertical stress increment can be obtained through data fitting, as expressed in Eq. (7). The above equations provide a method for determining the collapsible modulus in the numerical simulation of collapsible deformation of tunnel loess strata.

$$\varepsilon_{sh} = 0.24\Delta p^5 - 1.1\Delta p^4 + 1.9\Delta p^3 - 1.5\Delta p^2 + 0.5\Delta p + 0.013 \tag{7}$$

Numerical simulations of the mechanical responses of a hydraulic tunnel in the collapsible stratum

Numerical computation scheme

Geometric model

Numerical simulation of water conservancy tunnel section size. According to the section of shield tunnel in Shenheyuan Highland of the second phase of the water diversion project from the Han River to the Wei River, the section of shield tunnel in Shenheyuan Highland is simulated (Kang et al. 2022). The three-dimensional geometric model of the hydraulic tunnel is established in FLAC3D, as shown in Fig. 5. The dimensions of the model are 50 m×180 m×50 m (X×Y×Z). The shield machine has a length of 7.5 m, and the outer diameter of the lining D is 5.2 m, with a thickness of 0.4 m. The tunnel cover has a depth of 10 m. The left and right boundaries of the model, starting from the tunnel edge to extend 4D. The surrounding rock and soil, excavated soil, collapsible soil, equivalent layer, and shield segments are simulated with solid elements. The shield machine is represented by shell elements, and the contact between the segments and surrounding rock is simulated with lining elements. The equivalent layer has a thickness of 0.12 m (Zhu et al. 2022). Each segment has a length of 1.5 m.

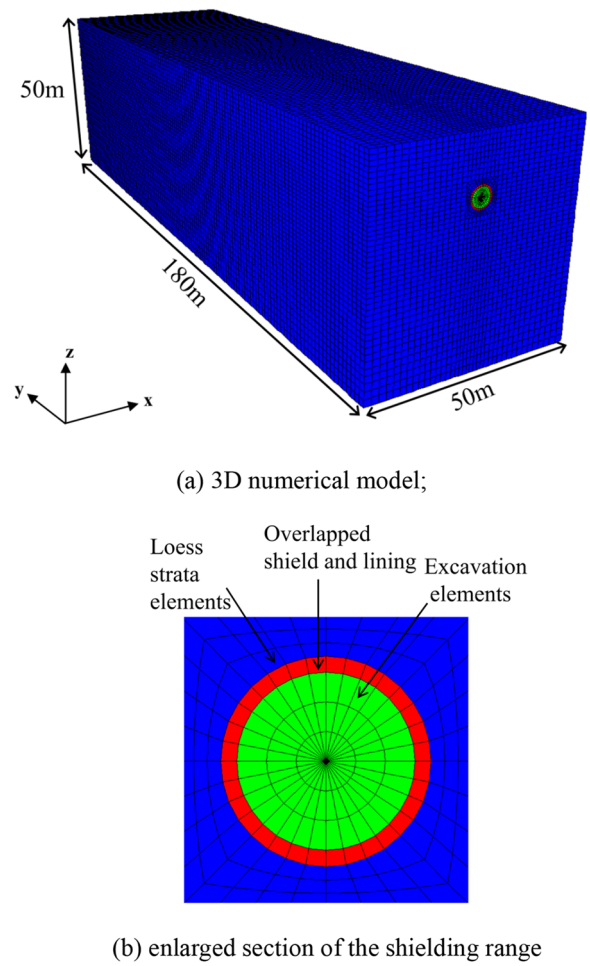

Fig. 5 Geometric mode

Model parameters

Based on the laboratory test data and relevant literatures (Zhu et al. 2022; Zhang et al. 2002), the simulation material parameters for the shield machine are determined and presented in Table 2. The constitutive model for the stratum material, including the collapsible loess stratum, is the Mohr–Coulomb ideal elastoplastic model. The shield machine is simulated by the elastic model of shell elements. The concrete segment adopts a linear elastic constitutive model for solid elements (Liu et al. 2017). The equivalent layer is modeled with the Mohr–Coulomb model.

Table 2 Physical and mechanical parameters for numerical computation

Soil type	Element type	Unit weight γ (kN/m^3)	Cohesion c (kPa)	Internal friction angle φ (°)	Elastic modulus E (MPa)	Poisson's ratio v
Natural loess	Entity	16.0	79	24.8	16	0.30
Saturated loess	Entity	18.5	29	21.6	11	0.35
Lining	Entity	25.0	–	–	34,500	0.15
Shield machine	Shell	78.0	–	–	206,000	0.28
Equivalent layer	Lining	21.0	–	–	300	0.20

Simulation method

The procedure for numerical simulation is illustrated in Fig. 6, which includes five main steps. The tunnel construction process is simulated based on the practical stratum condition and excavation method. It includes the identification of the initial stress σ_{zo} of surrounding rock immediately after excavation and modeling the collapsible deformation layer by layer within the collapsible domain. The first step is to calculate the stress increment Δp by subtracting the initial vertical stress σ_z of the free site of the soil element from the vertical stress σ_{zo} of the surrounding rock. The second step is to express the variation of the collapsibility coefficient δs for each depth of the soil layer that is obtained by laboratory tests as a function of the stress increment Δp. This function is then compiled into a program. The theoretical values of the stress increment Δp and the collapsibility coefficient δ_s for each soil element in the collapsible domain are

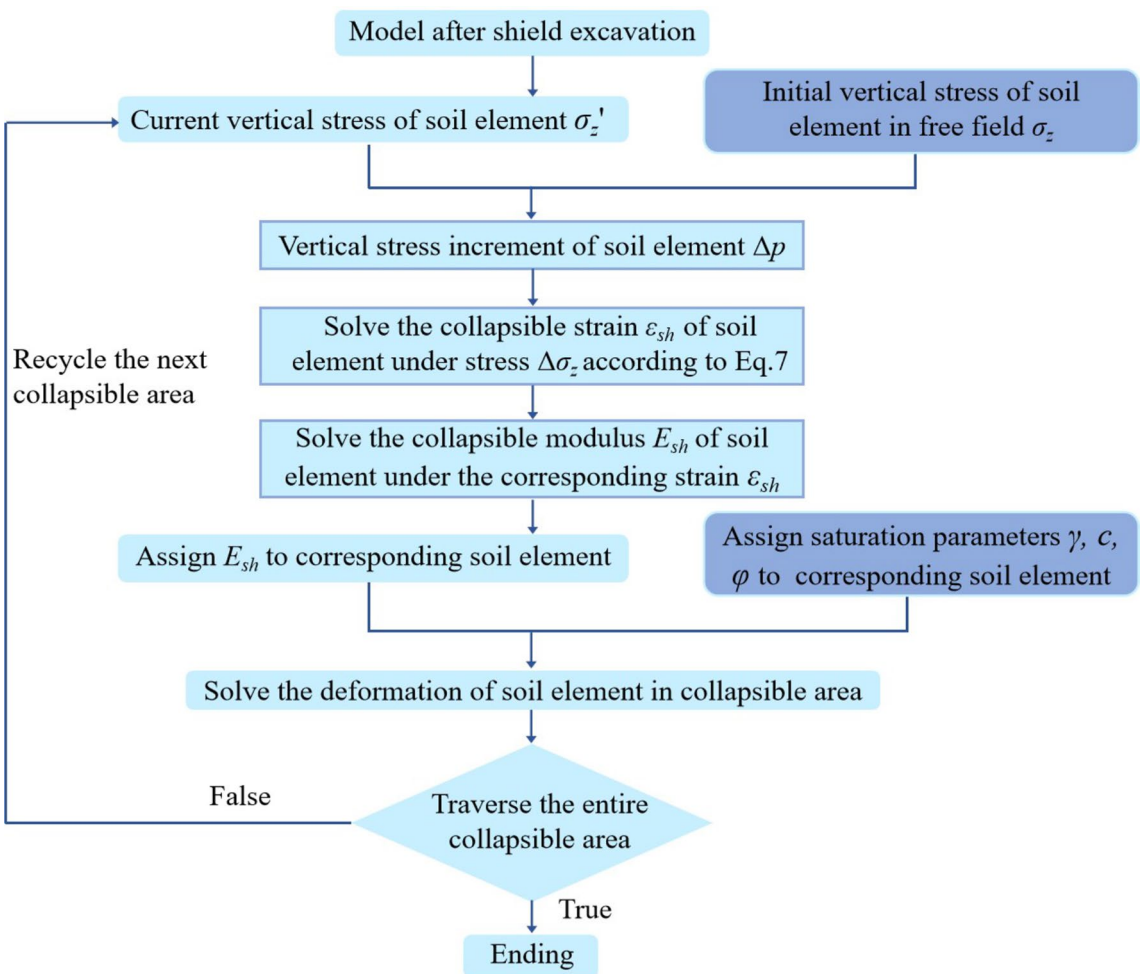

Fig. 6 Computational procedure for the collapse of surrounding rock of a hydraulic tunnel

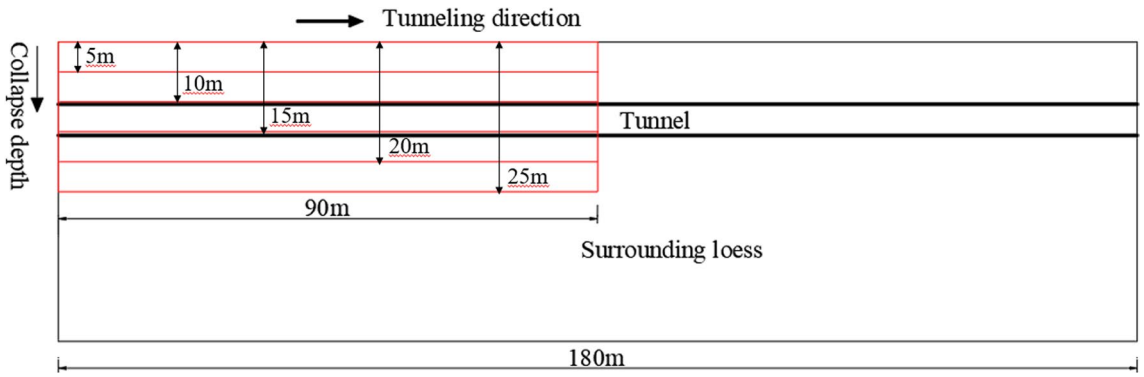

Fig. 7 Longitudinal section of collapsibility

determined based on the current stress state. The third step is to calculate the collapsible secant modulus E_{sh} corresponding to the collapsibility coefficient δ_s of each collapsible soil element under the vertical stress increment Δp. Additionally, the actual compression modulus E_{sh} of the collapsible stratum is calculated in the fourth step. In the fifth step, the elastic modulus E_{sh} and the basic parameters for saturated soil elements, such as specific gravity γ, cohesion c, and internal friction angle ϕ are incorporated into the corresponding collapsible soil element to calculate the additional deformation. After completing the collapsibility calculation for each layer, the calculation cycle is repeated for the lower layers until the collapsibility of the entire preset soaking area is accounted for (Fig. 7).

Figure 8 illustrates a schematic diagram of different immersion areas. During the simulation of the immersion collapsibility process, the front half of the model collapses along the longitudinal direction (Y direction), while the latter half remains untreated for comparison purposes. The numerical simulation is conducted for five different working conditions, specifically at distances of 5 m, 10 m, 15 m, 20 m, and 25 m, wherein the red box represents the area of collapsible loess.

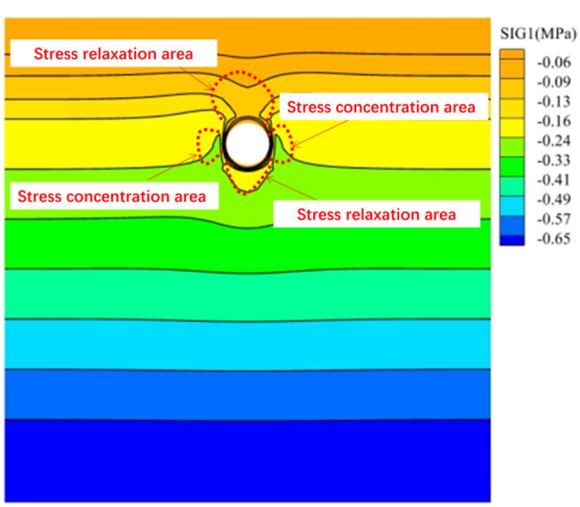

Fig. 8 Vertical stress distribution of tunnel surrounding rock after shield excavation. (*Note*: SIG1 indicates the vertical stress of the tunnel foundation, and the negative sign is the compressive stress)

Result analysis

Vertical stress distribution of hydraulic tunnel

Figure 8 presents the profile of the vertical stress of the tunnel surrounding rock after shield excavation. It can be seen that the stress is redistributed around the tunnel lining, and the stress relaxation area appears in the surrounding rock at the top and bottom of the tunnel, where the stress is lower than the ground stress. The stress concentration area appears in the surrounding rock at the middle of the tunnel, where the stress is greater than the ground stress. Because the coefficient of loess collapsibility changes with the stress increment (i.e., the difference between the stress of the tunnel surrounding rock and the stress of natural ground), the difference in stress distribution of surrounding rock will cause the change of collapsible deformation.

Collapsible deformation of the strata

Figure 9 presents the settlement contour of the tunnel surrounding rock with different collapsible depths. When the collapsible depth is 5 m, the ground settlement within 5 m of the ground surface is primarily caused by collapsible deformation. Below 5 m, the settlement is attributed to compressive deformation which results from the increase in the unit weight after soaking. Thus, after the surrounding rock is soaked, the soil deformation is mainly the collapsible and compressive deformation. The settlement of the surrounding rock is relatively small in the middle and larger on both sides. This discrepancy is primarily caused by the difference

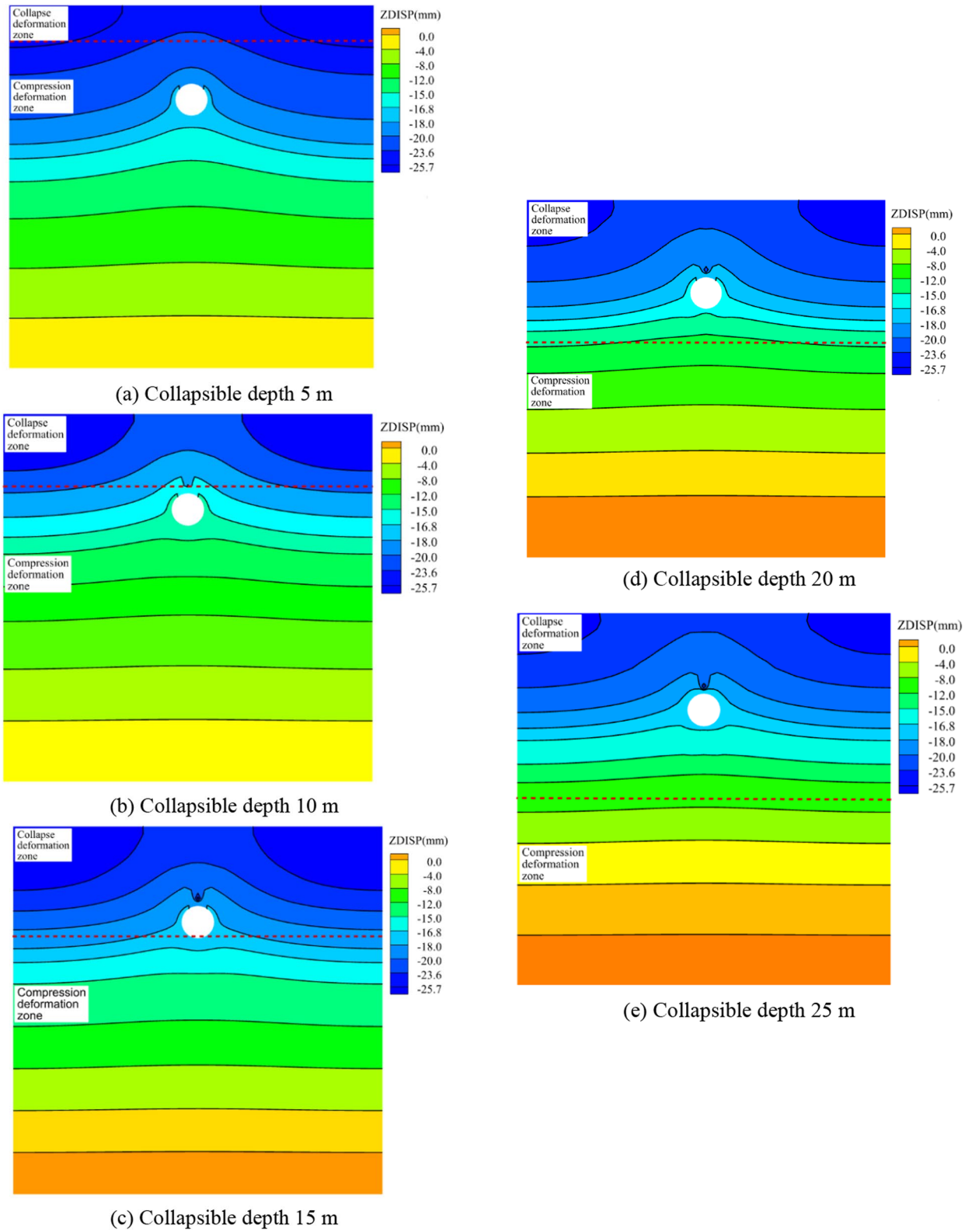

Fig. 9 Settlement contour of tunnel surrounding rock with different collapsible depth. (*Note*: ZDISP represents the vertical displacement of the tunnel foundation, and the negative sign is the settlement displacement.)

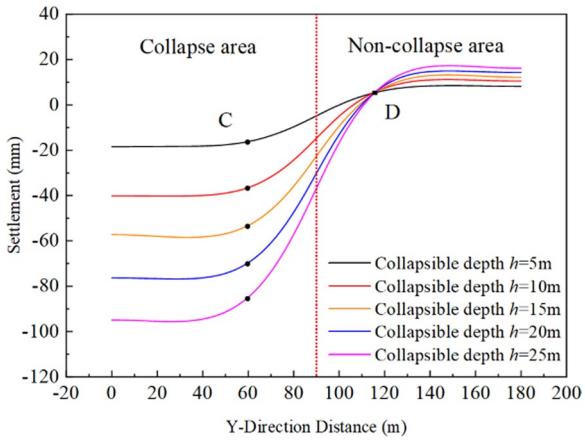

Fig. 10 Settlement of lining structure with different collapsible thicknesses along the longitudinal axis

in stiffness between the tunnel lining structure and the soil. When the collapsible depth reaches 20 m, the entire tunnel lining structure is within the collapsible domain. However, the collapsible deformation of the soil near the bottom of the tunnel is smaller compared to other areas at the same depth. This phenomenon is due to the smaller collapsible deformation resulting from stress relaxation at the bottom of the tunnel.

Deformation of lining structure

Figure 10 presents the deformation of the lining structure with varying collapsible thicknesses. The maximum settlement of the lining structure increases as the collapsible depth increases, leading to an increase in differential settlement of the lining. Along the longitudinal settlement, the maximum curvature position of the lining structure occurs at point C, which is 30 m away from the center line within the collapsible area. In contrast, within the non-collapsible area, the maximum curvature position is at point D, located 25 m away from the center line.

Stress of lining structure

The major and minor principal stresses of the lining structure are positive in tension and negative in compression. The large principal stress primarily represents the tensile characteristics of the tunnel lining structure, while the small principal stress predominantly reflects the compressive characteristics of the lining structure. Figures 11 and 12 present the profiles of tensile stress and compressive stress, respectively within the lining structure at different collapsible depths. The profiles show that the loess

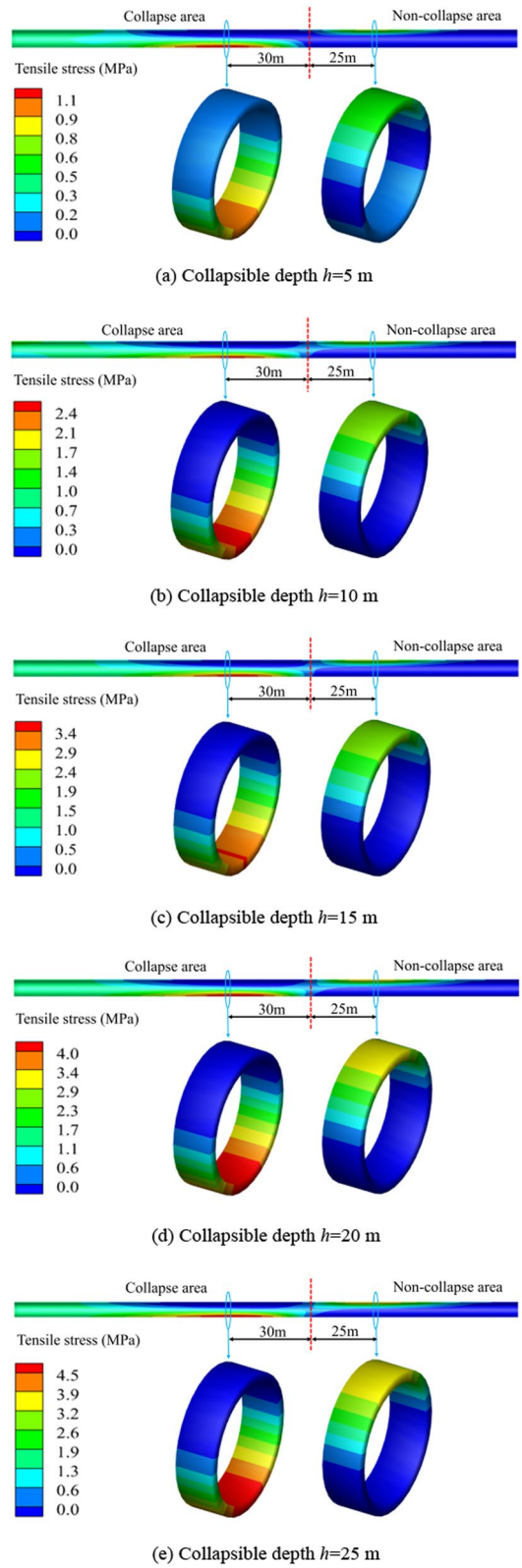

Fig. 11 Distribution of tensile stress of tunnel lining structure

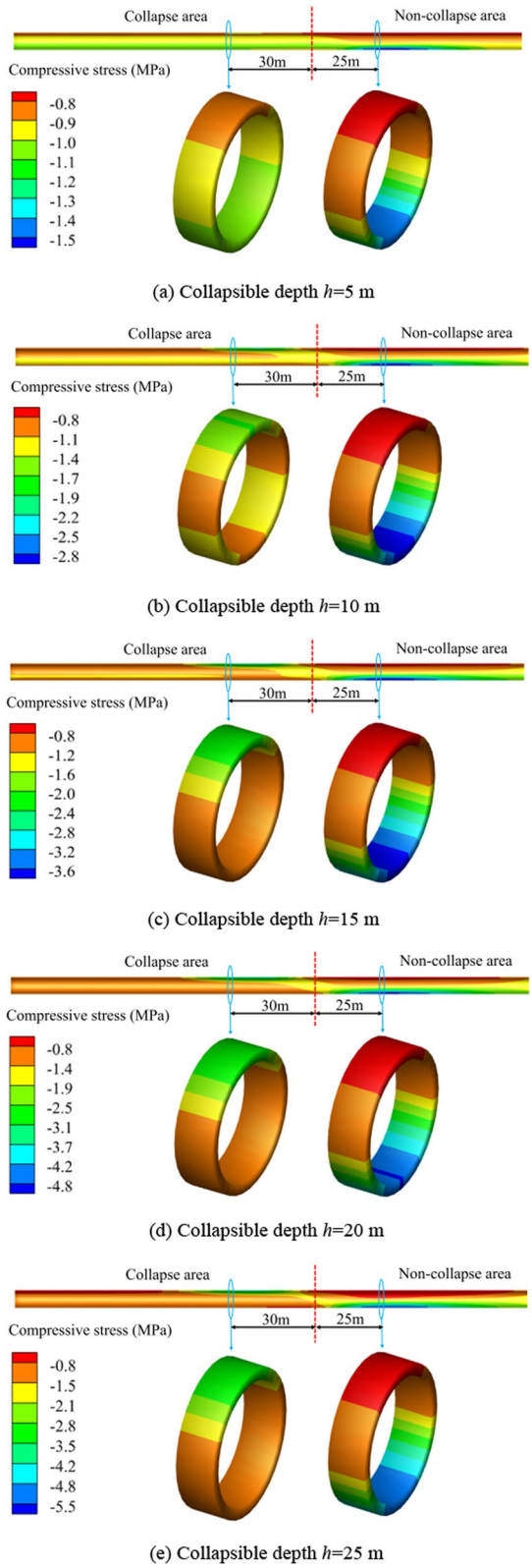

Fig. 12 Distribution of compressive stress of tunnel lining structure

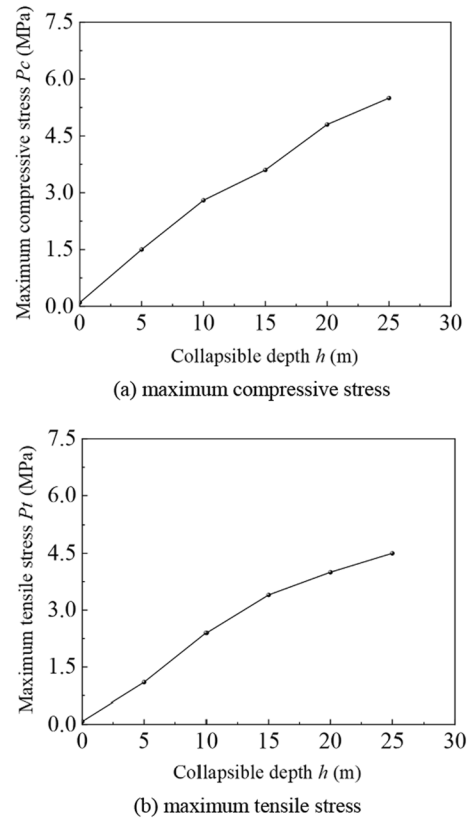

Fig. 13 Variation of maximum principal stress of lining structure with collapsible depth

collapsibility leads to significant and uneven settlement of the lining structure, resulting in stress concentration. The maximum tensile stress and compressive stress of the lining structure in the collapsible area and non-collapsible area are at the maximum curvature position of the lining structure along longitudinal settlement. The maximum tensile stress and the maximum compressive stress of the tunnel lining structure occur at the bottom and the top of the tunnel lining structure in the collapsible area, respectively. In Fig. 13, the maximum stress of the lining structure changes with collapsible depth, indicating that the tensile stress and compressive stress of the lining structure exhibit a linear increase with collapsible depth.

Stress of the surrounding rock

Figure 14 presents the stress contour of the tunnel surrounding rock with different collapsible depths. It can be seen that the stress distribution law of surrounding rock with different collapsible depths is the same, and it is consistent with the stress distribution after tunnel excavation, as shown in Fig. 8. However, when the collapsible area is directly above the tunnel, with the

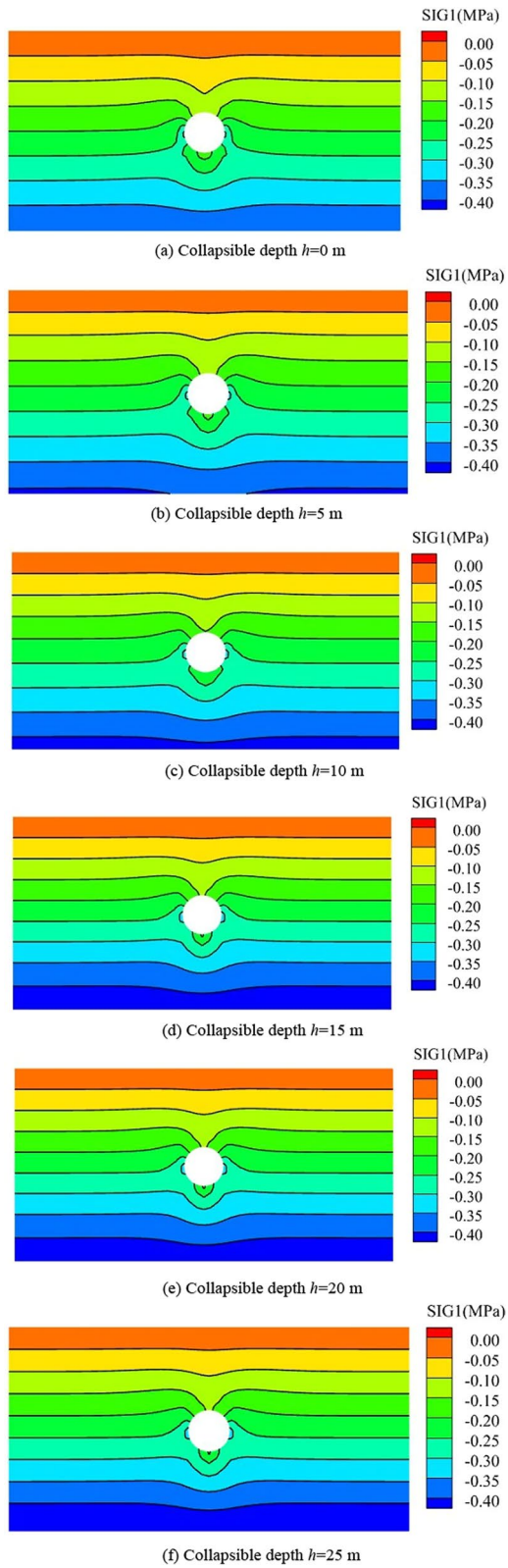

Fig. 14 Stress contour of tunnel surrounding rock with different collapsible depth. (*Note*: SIG1 indicates the vertical stress of the tunnel foundation, and the negative sign is the compressive stress)

increase of the collapsible area, the stress of the surrounding rock at the vault of the tunnel increases obviously. When the tunnel is completely immersed in the collapsible area, with the increase of the collapsible area, the stress of the surrounding rock at the vault of the tunnel no longer changes, and the stress of the surrounding rock under the inverted arch of the tunnel increases. The application of unsaturated area is the unit weight of unsaturated loess. On this basis, the application of collapsible area is the increment of unit weight of saturated and unsaturated loess.

Conclusions

In this study, the influence of loess collapsibility on the mechanical responses of a hydraulic tunnel was analyzed considering the relationship between loess collapsible deformation and vertical stress. The confined compression tests and the double-line method were adopted to evaluate the loess collapsibility. Besides, a three-dimensional numerical model of the hydraulic tunnel is established to investigate the deformation of the surrounding rock and its impact on the stress profile of the lining structure which considers varying ground stress. The main conclusions drawn from this study are as follows:

(1) The relationship between the collapsibility coefficient and vertical stress can be divided into three stages: linear increase, nonlinear increase, and nonlinear decrease. The critical point between the former two stages corresponds to the preconsolidation pressure of saturated soil. Likewise, the critical point for the latter two stages corresponds to the structural yield pressure of unsaturated soil.
(2) The deformation of the tunnel during infiltration is divided into two types: collapsible and compressive deformation. When the infiltration depth is shallow, the deformation near the lining is primarily due to compression. However, as the infiltration reaches the bottom of the tunnel invert, the deformation near the tunnel lining originates from both collapsible and compressive deformation. The excavation of the tunnel causes stress relaxation in the soil near the lining. This stress relaxation results in a smaller collapsibility deformation compared to the initial stratum.
(3) The tensile stress and compressive stress of the tunnel lining structure increase linearly with the increase of the collapsible depth. The maximum tensile stress and compressive stress of the lining appear at the maximum curvature position of

the longitudinal settlement of the lining structure. The maximum stress of the lining in the collapsible area is 30 m away from the midline while that in the non-collapsible area is 25 m away. Therefore, the lining structure of the water conservancy tunnel in the collapsible loess stratum should be improved by increasing the reinforcement ratio and the concrete grade at the vault and arch bottom.

Author contributions

SF is responsible for establishing the research framework and making revisions to the paper. XW primarily focuses on conducting experiments and writing the corresponding sections. LL performs numerical simulations. LG and DC provides engineering data for the experiments. LL collects the soil samples used in the experiments. Both authors read and approved the final manuscript.

Funding

This research is financially supported by the National Natural Science Foundation of China (No. 51608442) and the Basic Research Program of Natural Science of Shaanxi Province (No. 2019JLM-56). These supports are greatly appreciated.

Availability of data and materials

All data, models, and code generated or used during the study appear in the submitted article.

Declarations

Competing interests

The authors declare that they have no competing interests.

Received: 13 July 2023 Accepted: 7 November 2023
Published online: 15 November 2023

References

Derbyshire E (2001) Geological hazards in loess terrain with particular reference to the loess areas of China. Earth-Sci Rev 54(1–3):231–260. https://doi.org/10.1016/S0012-8252(01)00050-2

Derbyshire E, Meng XM et al (1995) Collapse loess on the Loess Plateau of China. In: Derbyshire E, Dijkstra T, Smalley IJ (eds) Genesis and properties of collapsible soils. Kluwer, Dordrecht, pp 267–293. https://doi.org/10.1007/978-94-011-0097-7_14

Haeri SM, Khosravi A, Garakani AA et al (2017) Effect of soil structure and disturbance on hydromechanical behavior of collapsible loessial soils. Int J Geomech 17(1):04016021. https://doi.org/10.1061/(ASCE)GM.1943-5622.0000656

Haeri SM, Garakani AA, Roohparvar HR (2019) Testing and constitutive modeling of lime-stabilized collapsible loess. I: experimental investigations. Int J Geomech. https://doi.org/10.1061/(ASCE)GM.1943-5622.0001364

Houston SL, Houston WN, Spadola DJ (1988) Prediction of field collapse of soils due to wetting. J Geotech Eng 114(1):40–58. https://doi.org/10.1061/(ASCE)0733-9410(1988)114:1(40)

Jin X, Wang TX, Zhnag Y et al (2021) A modulus reduction method for calculating loess unloading collapse. Chin J Rock Mech Eng 40(07):1473–1483. https://doi.org/10.13722/j.cnki.jrme.2020.0783. (**in Chinese**)

Kang K, Wang ZZ, Dong P et al (2022) Inversion analysis of surrounding rock permeability coefficient and external water load of shield tunnel in high groundwater complex stratum. J Water Resour Archit Eng 20(05):35–41 (**in Chinese**)

Li J (2007) Simulation of pile-soil interaction behavior of bridge pile in loess area and its test study. Chin J Rock Mech Eng 198(05):1081–1590 (**in Chinese**)

Li P, Vanapalli S, Li TL (2016a) Review of collapse triggering mechanism of collapsible soils due to wetting. J Rock Mech Geotech Eng 8(02):256–327

Li P, Jiao ZH, Jiao X (2016b) Discussion on the evaluation of loess collapsibility in the water diversion line in Guanzhong area-taking the north main line of the second phase of Hanjiang-to-Weihe River Water Diversion Project as an example. Resour Environ Eng 30(03):429–432. https://doi.org/10.16536/j.cnki.issn.1671-1211.2016.03.042. (**in Chinese**)

Li J, Shao SJ, Shao S (2019) Collapsible characteristics of loess tunnel site and their effects on tunnel structure. Tunn Undergr Space Technol 83:509–519. https://doi.org/10.1016/j.tust.2018.08.035. (**in Chinese**)

Liu BJ, Xie DY, Guo ZY (2004) A practical algorithm for humidifying deformation of loess found loess ation. Rock Soil Mech 2004(02):270–274. https://doi.org/10.16285/j.rsm.2004.02.025. (**in Chinese**)

Liu B, Zhang DW, Liu SY et al (2017) Numerical simulation and field monitoring on a large cross-section pipe-jacking underpass traversing existing metro tunnels. Chin J Rock Mech Eng 36(11):2850–2860. https://doi.org/10.13722/j.cnki.jrme.2017.1214

Ministry of Housing and Urban-Rural Development of the People's Republic of China (2018) Code for building construction in collapsible loess regions (GB 50025-2018). China Building Industry Press, Beijing (**in Chinese**)

Ministry of Housing and Urban-Rural Development of the People's Republic of China (2019) Code for geotechnical testing method (GB/T 50123-2019). China Building Industry Press, Beijing (**in Chinese**)

Reznik YK (2007) Influence of physical properties on deformation characteristics of collapsible soils. Eng Geol 92(1–2):27–37. https://doi.org/10.1016/j.enggeo.2007.03.001

Shao SJ, Yang CM, Jiao YY et al (2013) Engineering properties of collapsible loess tunnel. Chin J Geotech Eng 35(9):1580–1590 (**in Chinese**)

Shao SJ, Chen F, Shao S (2017) Collapse deformation evaluation method of loess tunnel foundation. Chin J Rock Mech Eng 36(5):1289–1300 (**in Chinese**)

Sharma RS, Singhal S (2012) Preliminary observation on volumetric behavior of unsaturated collapsible loess. Unsaturated Soils 2006:1027–1024. https://doi.org/10.1061/40802%28189%2982

Smalley IJ, Jefferson IF, Dijkstra TA et al (2001) Some major events in the development of the scientific study of loess. Earth Sci Rev 54(1–3):5–18. https://doi.org/10.1016/S0012-8252(01)00038-1

Su LN (2019) Study on the characteristics of collapsible loess in the second phase tunnel project of Yintao in Gansu Province. Ground Water 44(04):251–253 (**in Chinese**)

Umar M, Sadrekarimi A (2016) Accuracy of determining pre-consolidation pressure from laboratory tests. Can Geotech J 54(3):441–450. https://doi.org/10.1139/cgj-2016-0203

Weng XL, Sun YF, Zhang YW et al (2019) Physical modeling of wetting-induced collapse of shield tunneling in loess strata. Tunn Undergr Space Technol 90:208–219. https://doi.org/10.1016/j.tust.2019.05.004

Weng XL, Zhou RM, Rao W et al (2021) Research on subway shield tunnel induced by local water immersion of collapsible loess. Nat Hazards 108:1197–1219. https://doi.org/10.1007/s11069-021-04727-4

Xiao QL, Tang DL (2013) Humidification deformation characteristics and collapsible calculation method of loess. J China Foreign Highw 33(04):54–57. https://doi.org/10.14048/j.issn.1671-2579.2013.04.085. (**in Chinese**)

Xiao QH, Lei SX, Cui K et al (2022) Effect of the longitudinal local wetting-induced collapse on tunnel structure in loess strata. Tunn Undergr Space Technol. https://doi.org/10.1016/j.tust.2022.104361

Yuan H, Xin YP, Yu XL (2017) FLAC3D simulation of the influence of loess collapsibility on subgrade settlement. Highw Traffic Technol (appl Technol Ed) 13(08):158–159 (**in Chinese**)

Zhang Y, Yin ZZ and Xu YF, (2002) Analysis of ground deformation caused by shield tunneling. Chin J Rock Mech Eng 3:388–392

Zhao WT (2019) Research on foundation treatment depth of shanxi deep collapsible loess venues. In: Proceedings of the symposium on new materials, new technologies and their engineering applications in civil engineering, volume II, pp 1372–1375. https://doi.org/10.26914/c.cnkihy.2019.046404 (**in Chinese**)

Zhi B, Wei PP, Wang XC et al (2021) Research on the collapse coefficient of collapsible loess under unloading. Adv Civ Eng. https://doi.org/10.1155/2021/6672301

Zhu CH, Wang S, Peng S et al (2022) Surface settlement in saturated loess stratum during shield construction: numerical modeling and sensitivity analysis. Tunn Undergr Space Technol. https://doi.org/10.1016/j.tust.2021.104205

Publisher's Note